Journal of Taibah University Medical Sciences (2023) 18(5), 933–946

Taibah University

Journal of Taibah University Medical Sciences

www.sciencedirect.com

Original Article

Virtual screening, pharmacokinetic, and DFT studies of anticancer compounds as potential *V600E-BRAF* kinase inhibitors

Abdullahi B. Umar, PhD * and Adamu Uzairu, PhD

Department of Chemistry, Faculty of Physical Sciences, Ahmad Bello University, Zaria, Nigeria

Received 19 September 2022; revised 12 December 2022; accepted 24 January 2023; Available online 4 February 2023

المخلص

أهداف البحث: كيناز "ب.ر.أ. ف-في. 600.إي". هو هدف علاجي أساسي في سرطان الجلد وأنواع أخرى من الأورام. تستلزم مقاومته للمثبطات والآثار الجانبية المعروفة لبعض المثبطات المحددة الاستقصاء عن مثبطات جديدة وفعالة.

طرق البحث: في العمل الحالي، تم استخدام استراتيجيات في السيليكون مثل محاكاة الالتحام الجزيئي وتقييم الحرائك الدوائية وحسابات نظرية الكثافة الوظيفية لتحديد مثبطات "ب.ر.أ. ف-في. 600.إي" المحتملة من مجموعة من 72 مركبا مضادا للسرطان من قاعدة بيانات "بوبكيم".

النتائج: ما مجموعه خمسة جزيئات من الدرجة الأولى (12 ، 15 ، 30 ، 31 ، 35) مع درجات رائعة في الالتحام (درجة مولدوك:> 90 كيلو كالوري مول -1 ، ونقاط إعادة التصنيف:> 60 كيلو كالوري مول -1) تم اختيارها. تم اكتشاف العديد من تفاعلات الارتباط المحتملة بين الجزيئات المقترحة و "ب.ر.أ. ف-في. 600.إي". أثبت ظهور الروابط الهيدروجينية والتفاعلات الكارهة للماء مع المخلفات الأساسية لـ "ب.ر.أ. ف-في. 600.إي" الثبات العالي لهذه المجمعات. أظهرت المركبات المختارة خصائص دوائية فائقة وفقا لقواعد التشابه الدوائي (التوافر البيولوجي) وخصائص الحرائك الدوائية. وبالمثل، تم حساب الطاقة الخاصة بالمدارات الجزيئية الحدودية مثل المدار الجزيئي الأعلى المشغول، وأدنى المدار الجزيئي غير المشغول، وفجوة الطاقة، ومعلمات التفاعل الأخرى باستخدام نظرية الكثافة الوظيفية. تم فحص الأسطح المدارية الجزيئية الحدودية والإمكانات الكهروستاتيكية لإثبات توزيعات كثافة الشحنة التي قد تكون مرتبطة بالنشاط المضاد للسرطان.

الاستنتاجات: وبالتالي، تم التعرف على المركبات المختارة كضربات قوية لـ "ب.ر.أ. ف-في. 600.إي". بخصائص حركية دوائية فائقة، ويمكن اقتراحها كعقاقير مرشحة واعدة للسرطان.

الكلمات المفتاحية: ب.ر.أ. ف-في. 600.إي؛ الالتحام الجزيئي؛ شبيه-الدواء؛ نظرية الكثافة الوظيفية؛ امتصاص وتوزيع وتمثيل الدواء وإفرازه وسميته.

Abstract

Objectives: *V600E-BRAF* kinase is an essential therapeutic target in melanoma and other types of tumors. Because of its resistance to known inhibitors and the adverse effects of some identified inhibitors, investigation of new potent inhibitors is necessary.

Methods: In the present work, in silico strategies such as molecular docking simulation, pharmacokinetic evaluation, and density functional theory (DFT) computations were used to identify potential *V600E-BRAF* inhibitors from a set of 72 anticancer compounds in the PubChem database.

Results: Five top-ranked molecules (12, 15, 30, 31, and 35) with excellent docking scores (MolDock score $\geq$90 kcal mol^{-1}, Rerank score $\geq$60 kcal mol^{-1}) were selected. Several potential binding interactions were discovered between the molecules and *V600E-BRAF*. The formation of H-bonds and hydrophobic interactions with essential residues of *V600E-BRAF* suggested the high stability of these complexes. The selected compounds had excellent pharmacological properties according to the drug likeness rules (bioavailability) and pharmacokinetic properties. Similarly, the energy for the frontier molecular orbitals, such as the HOMO, LUMO, energy gap, and other reactivity parameters, was computed with DFT. The frontier molecular orbital surfaces and electrostatic potentials were investigated to demonstrate the charge-density distributions potentially associated with anticancer activity.

* Corresponding address: Department of Chemistry, Faculty of Physical Sciences, Ahmad Bello University, Zaria, P.M.B.1045 Kaduna State, Nigeria

E-mail: abdallahbum@yahoo.com (A.B. Umar)

Peer review under responsibility of Taibah University.

ELSEVIER Production and hosting by Elsevier

 https://doi.org/10.1016/j.jtumed.2023.01.013

Conclusion: The identified compounds were found to be potent hit compounds for *V600E-BRAF* inhibition with superior pharmacokinetic properties; therefore, they may be promising cancer drug candidates.

Keywords: ADMET; DFT; Drug likeness; Molecular docking; *V600E-BRAF*

Introduction

MAPK signaling is a key regulator of fundamental cellular processes such as growth, proliferation, differentiation, migration, and apoptosis.[1,2] Signal transmission is enabled by intracellular protein kinase phosphorylation cascades (e.g., *MAPK, MKKK,* and *MKK*).[3] The abnormal regulation of MAPK cascades is associated with the onset of a variety of severe diseases, including Parkinson's disease, Alzheimer's disease, amyotrophic lateral sclerosis, and multiple types of cancer.[4,5] Disruption of the *Ras-Raf-MEKERK* signaling pathway has been associated with human tumorigenesis.[6] *Raf* kinases (*A, B*, and *CRAF*) play important roles in the *ERK* signaling branch of the *MAPK* cascade.[7] *RAF* kinases bind *RAS*, the upstream activator, and mediate MAPK signaling transduction to MEK, thus activating downstream *MEK1*/2 and *ERK1*/*2*.[8,9] *BRAF* has the highest basal activity among the three *RAF* kinases and is a key activator of *MEK1*/*2*. In comparison to *A* and *CRAF*,[10,11] pathological mutations in RAF kinases typically affect the BRAF subtype.[12] The most common mutation is *V600E-BRAF*, which occurs when the valine residue at position 600 is replaced with a glutamate residue.[13] Because this mutation mimics the active phosphorylation state, the *V600E-BRAF* protein continues to activate downstream pathways without being regulated.[14] This mutation is present in 8% of all cancers, such as colorectal cancer (10%), melanoma (60%), and thyroid cancer (30–70%).[15,16] Thus, *V600E-BRAF* kinase is considered an important target for managing and treating cancer.[17,18]

Dabrafenib and vemurafenib are both selective inhibitors of *V600E-BRAF*; they induce automatic cell death in melanoma and have shown high effectiveness against melanoma cells. They have been endorsed by the US Food and Drug Administration for late-stage melanoma therapy.[19,20] A single treatment with a *V600E-BRAF* inhibitor considerably improves patient lifestyle and survival rate. Unfortunately, despite the success of approved *V600E-BRAF* inhibitors, resistance to these selective inhibitors emerges after 5–8 months.[21,22] The resistance to selective *V600E-BRAF* inhibitors makes the discovery and validation of novel candidates critical for the development of new treatments for *V600E-BRAF* cancers. Moreover, current understanding of tumor heterogeneity and the evolution of resistance suggests that the development of novel anticancer agents is critical. In drug discovery, the identification and confirmation of lead compounds and the evaluation of active binding sites of bioactive targets linked with specific lead compounds is performed through wet-laboratory investigations, which are costly and time-consuming.[23] In silico strategies can effectively decrease the time needed to acquire valuable drugs and the accompanying financial costs, thus enabling new potent drugs to be identified with lower costs and selective targeting.[24] Molecular docking is an excellent in silico approach for filtering large chemical libraries to detect prospective chemicals that may be used to determine the binding ability for a certain target. Over the past two decades, molecular docking has evolved as a model for structure-based virtual screening of several chemical databases.[25] It is extensively used to select the most suitable alignment of a drug candidate in the active site of a protein, and to predict target affinity. Previously, comprehensive docking investigations were performed to study the biological activity of numerous chemical structures.[25–27] In silico drug-like and pharmacokinetic analyses are additional (virtual) screening methods for the approval of compounds that might demonstrate physiological and drug-like ability. The procedures used to assess drug likeness and pharmacokinetic properties are based on a combination of the experimental findings reported in several drug databases.[28] Density functional theory (DFT) is an extensive technique with lower computational costs than those of several other approaches. DFT computations currently produce the most reliable and accurate outcomes for various chemical systems, providing results well matched to experimental findings.[29] In this investigation, a systematic computational investigation of a set of 72 anticancer compounds from the PubChem database was conducted with molecular docking simulation, DFT computations, and pharmacokinetic property prediction to explore their potential to inhibit the *V600E-BRAF* kinase. The objective of the work was to assess the anticancer potential of these chemical structures as likely drug candidates with desirable properties.

Materials and Methods

Retrieval of compounds and optimization

A series of 72 anticancer compounds was retrieved from the PubChem database (https://pubch em.ncbi.nlm.nih.gov). Structures of ligands were drawn in ChemDraw (Table S1), and minimization of energy was achieved with the MM2 forcefield in Spartan 14 to assist the docking program in detecting the bioactive conformer from the local minima. Optimization of the compounds was achieved with the DFT/B3LYP approach and 6–31G* basis set.

Docking preparation and simulation

The Protein Data Bank (http://www.rcsb.org/) was used to obtain the crystal structure of *V600E-BRAF* (PDB code: 3OG7)[12,30,31] and the native ligand (vemurafenib). The target was prepared by extracting water molecules and detaching vemurafenib from the protein–ligand complex. The native ligand was re-docked to the target to validate the molecular docking with Molegro Virtual-Docker (MVD) 6.0.[32] The active site of the target was determined with a cavity detection package in MVD 6.0. The binding cavity of X:

1.59, Y: −1.28, Z: −6.2, and r: 28 Å was set with 0.30 Å resolution.[25,33] The prepared structures with vemurafenib were imported into MVD, and 1500 iterations were set for the docking algorithm. The docking simulation was run at least 50 times for each of the 10 poses, and the best poses were selected on the basis of predefined scoring functions.[34] Inter-molecular interactions of the selected poses were visualized with Discovery-Studio.

Drug-like and pharmacokinetic biochemical evaluation

Drug-like behavior of the selected compounds was investigated with SwissADME (www.swissadme.ch/), an online server, and pharmacokinetic parameters were examined with pkCSM (https://biosig.unimelb.edu.au/pkcsm//).

DFT computation

The structural and electronic properties of the four best compounds selected from the docking analysis were computed with DFT/B3LYP and the 6−31G* basis set in Spartan 14. The parameters calculated in this investigation are the energies of the frontier molecular orbitals (HOMO, LUMO, and energy gap) and other reactivity parameters: chemical hardness (η), softness (σ), electronegativity (χ) chemical potential (μ), and electrophilicity index (ω).[35] The electrostatic potential (EP) surfaces for the molecules were achieved from the population-analysis computations and displayed with Spartan 14. Consequently, the importance of ligand/protein interactions in the active site of the target were clarified. The flowchart of the study design for identifying potent *V600E-BRAF* inhibitors is presented in Figure 1.

Results

Molecular docking results of the compounds including vemurafenib are shown in Table S1. The superimposed alignments of the re-docked and original co-crystal ligands are presented in Fig. S1. The complete docking results for the

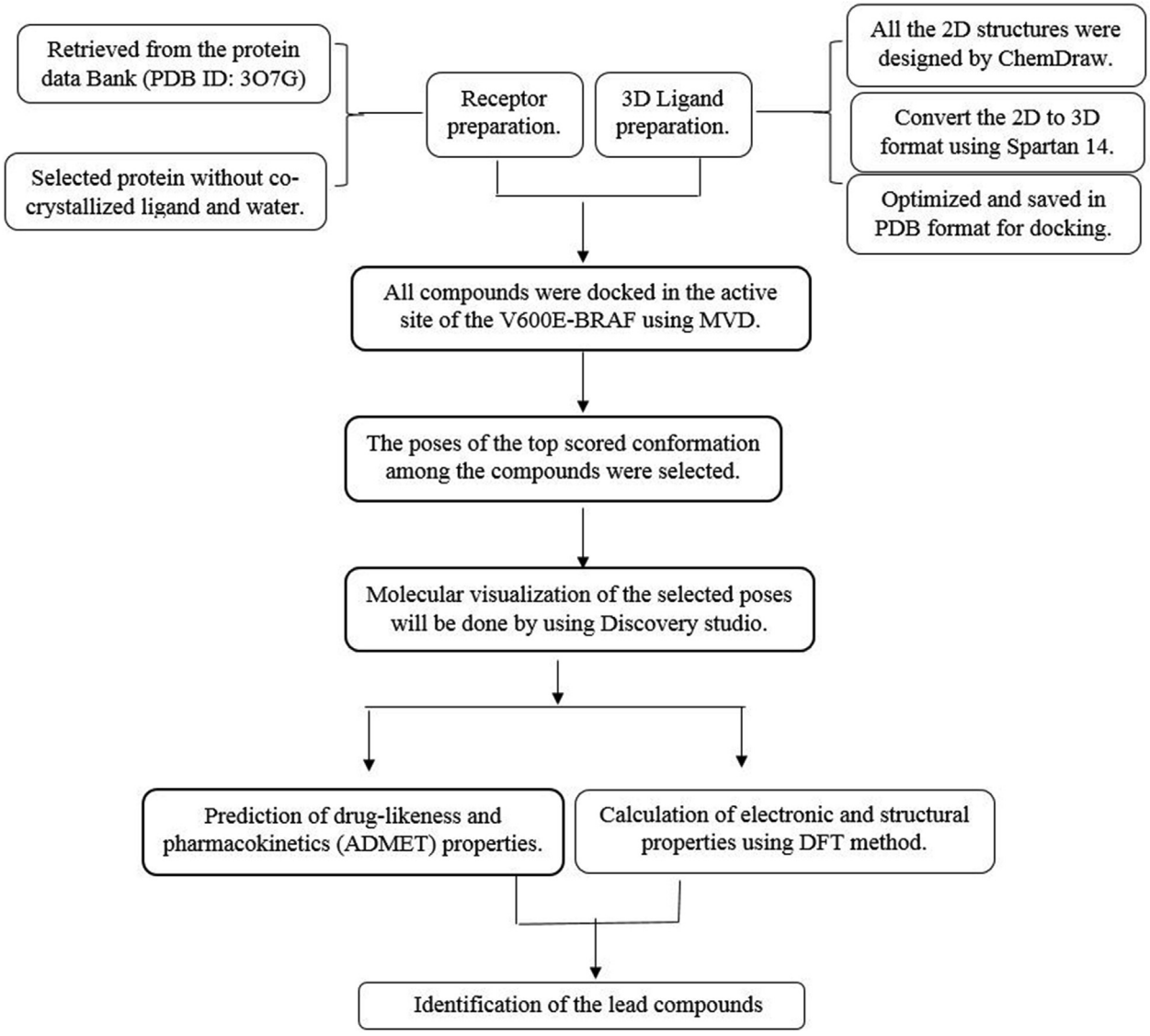

Figure 1: Flowchart of the study design for identifying potent *V600E-BRAF* inhibitors.

Table 1: Results of docking for the four best-docked ligands in *V600E-BRAF*.

SN	CID	Name	[a]MolDock score (kcal mol^{-1})	[b]Rerank score	[c]E-inter (kcal mol^{-1})	[d]E−H-bond (kcal mol^{-1})
12	72,742	Dermocybin	−139.140	−106.737	−149.917	−8.202
15	354,395	11-Hydroxymethyl-20(RS)-camptothecin	−116.449	−17.752	−133.922	−4.628
30	5,477,796	Anthra[1,9-cd]pyrazol-6(2H)-one der	−147.599	−115.756	−186.185	−4.770
31	5,351,180	Cytosine, monohydrochloride	−101.144	−76.975	−104.928	−9.939
35	5,351,321	Bisantrene hydrochloride	−134.615	−105.511	−152.904	−3.563
Vem.	–	Vemurafenib	−158.139	−118.607	−167.952	−4.741

CID, compound identification number; SN, serial number; Vem., vemurafenib.

Table 2: Interaction types and amino acids involved in each of the selected complexes.

Complex	H-bond (HB)	Bond length (Å) for HB	C−HB	Alkyl	π−alkyl	π−π	π−cation	π−sulfur	Halo-bond
12	CYS532	2.38906			VAL471	TRP531			
	CYS532	1.73263			ALA481	TRP531			
	CYS532	1.92474			LEU514	PHE583			
	GLN530	1.99728			CYS532				
	GLN530	1.6863			CYS532				
15	ASP594	2.34313	ASP594	VAL471	TRP531	TRP531		CYS532(s)	
	CYS532	2.09834			PHE583	PHE583			
	GLU533	2.65953			VAL471				
					ALA481				
					LYS483				
					LEU514				
					ALA481				
					CYS532				
30	LYS483	2.48979			VAL471	TRP531			
	ALA481	2.17008			ALA481	PHE583			
					VAL471	PHE583			
					ALA481	PHE583			
					CYS532				
31	LYS483	2.44902	LYS483		LEU505				
	ASP594	2.135			LEU514				
	ASP594	2.24205							
	PHE595	2.36902							
	GLY596	2.30303							
	THR508	2.9056							
	LEU514	1.96262							
	THR529	2.6848							
35	GLY534	1.64054	LYS483		VAL471	TRP531			
	CYS532	1.99523	GLY534		VAL471	PHE583			
			ILE527		ALA481	PHE583			
			ALA481		LEU514				
			THR529		CYS532				
			ALA481						
			ILE527						
Vem.	CYS532	1.788	GLY593	LEU505	VAL471	TRP531	LYS483		ALA481
	ASP594	1.980	CYS532	ILE527	LYS483	PHE583			
	GLN530	1.761	THR529		ALA481				
					LEU514				
					CYS532				
					ALA481				
					CYS532				

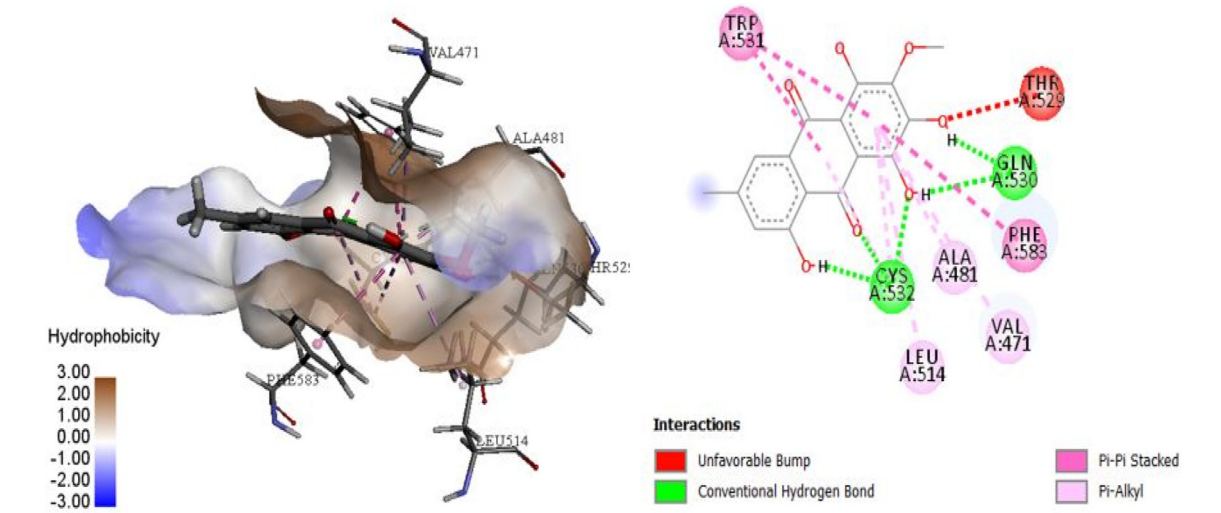

Figure 2: 3D and 2D models for the interaction of complex 12.

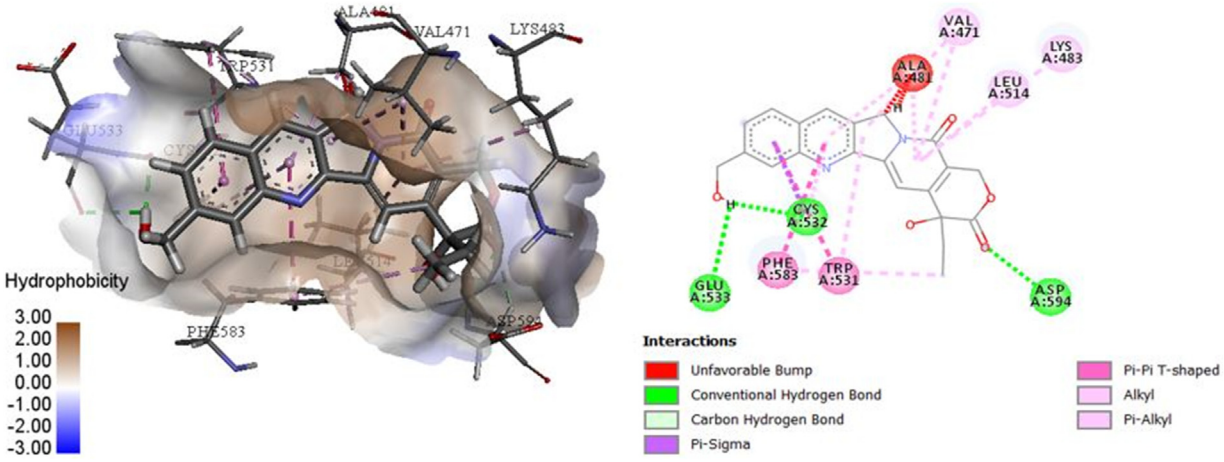

Figure 3: 3D and 2D models for the interaction of complex 15.

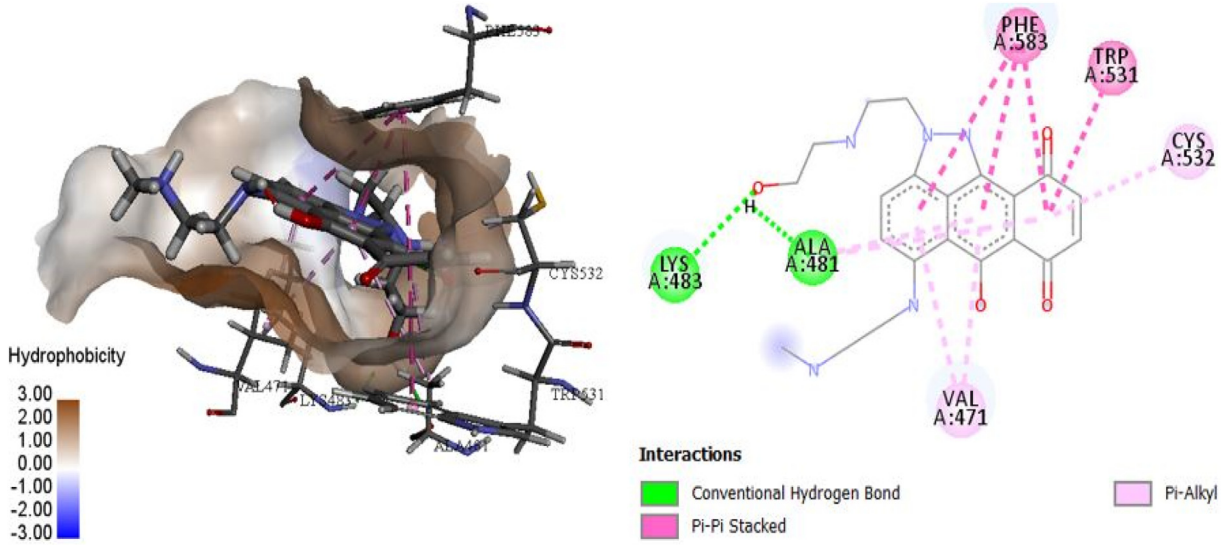

Figure 4: 3D and 2D models for the interaction of complex 30.

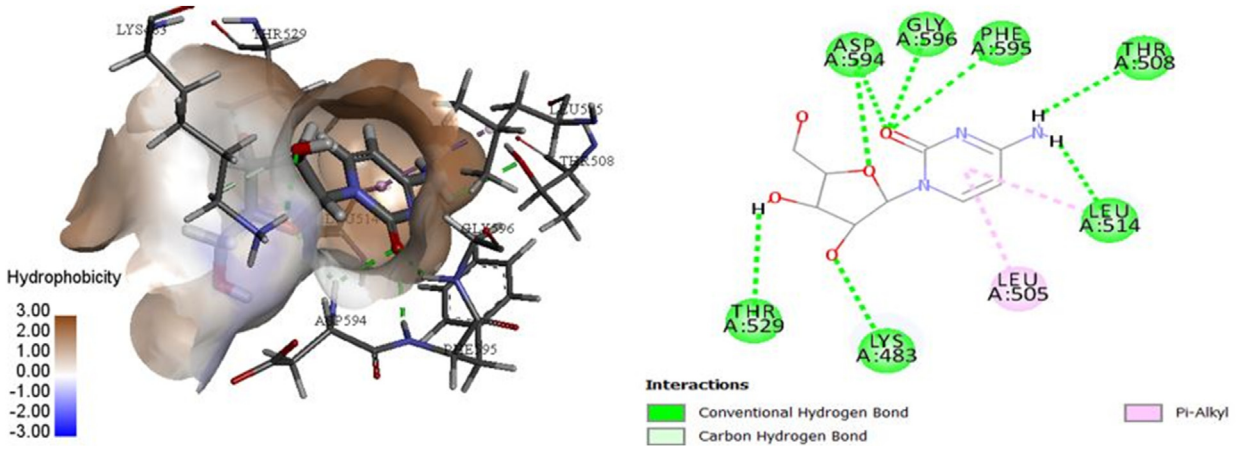

Figure 5: 3D and 2D models for the interaction of complex 3.

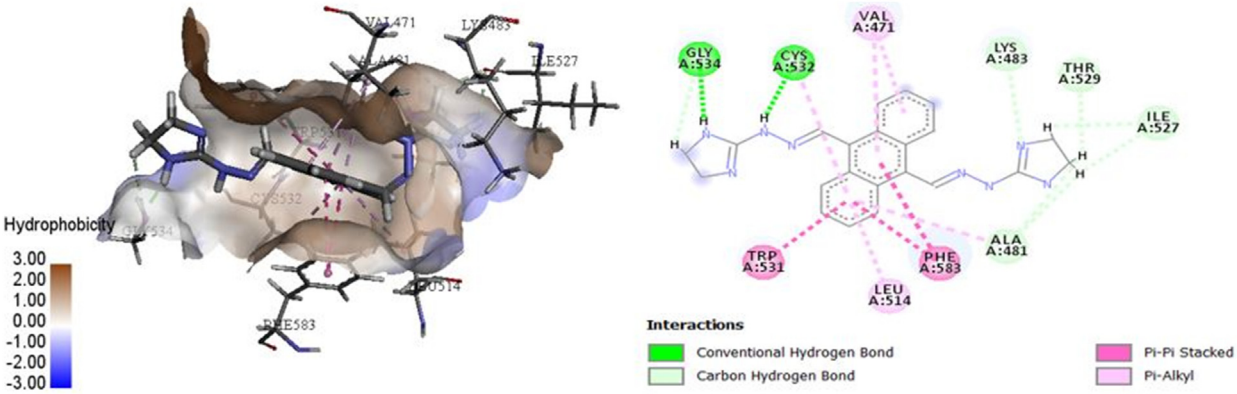

Figure 6: The 3D and 2D models for the interaction of complex 35.

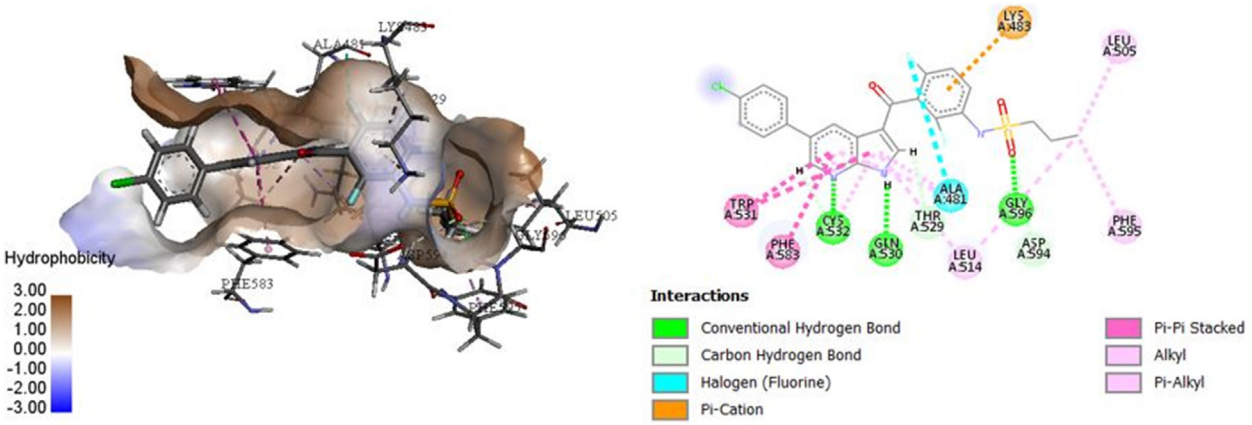

Figure 7: The 3D and 2D models for the interaction of the complex with vemurafenib.

Table 3: Predicted drug likeness parameters of the selected ligands.

SN	Mol. wt.	HBA	HBD	log P	NRB	TPSA (Å^2)	Bioavailability
12	316.26	7	4	2.15	1	124.29	0.55
15	378.38	6	2	2.56	2	101.65	0.55
30	453.49	7	5	3.33	11	137.48	0.55
31	243.22	6	4	0.32	2	130.83	0.55
35	398.46	4	4	2.71	6	97.56	0.55
Vem.	489.92	6	2	4.97	7	100.30	0.55

HBA, hydrogen bond acceptors; HBD, hydrogen bond donors; NRB, number of rotatable bond; SN, serial number; Vem., vemurafenib.

Table 4: Predicted pharmacokinetic properties of the selected ligands.

Absorption	Distribution				Metabolism							Excretion	Toxicity
					Substrate		Inhibitor						
					CYP								
SN	Intestinal absorption Numeric (% absorbed)	VDss (human) Numeric (log L kg^{-1})	BBB permeability Numeric (log BB)	CNS permeability Numeric (log PS)	2D6	3A4	1A2	2C19 (Yes/no)	2C9	2D6	3A4	Total clearance Numeric (log mL min^{-1} kg^{-1})	AMES toxicity (Yes/no)
12	87.842	0.201	0.152	−2.236	No	No	No	Yes	No	No	No	0.051	No
15	88.004	0.241	−0.584	−3.086	No	Yes	Yes	No	No	No	Yes	0.607	No
30	55.695	1.900	−1.689	−3.447	Yes	Yes	No	No	No	No	Yes	1.543	No
31	43.155	−0.025	−0.97	−4.023	No	No	No	No	No	No	No	0.562	No
35	80.488	1.483	−0.198	−2.482	No	Yes	Yes	No	No	Yes	No	0.496	Yes
Vem.	98.853	−0.445	−1.647	−3.463	No	Yes	No	Yes	Yes	No	Yes	0.132	No

BBB, blood−brain barrier; CNS, central nervous system; CYP, cytochrome P; VDss, volume distribution in a stable state.

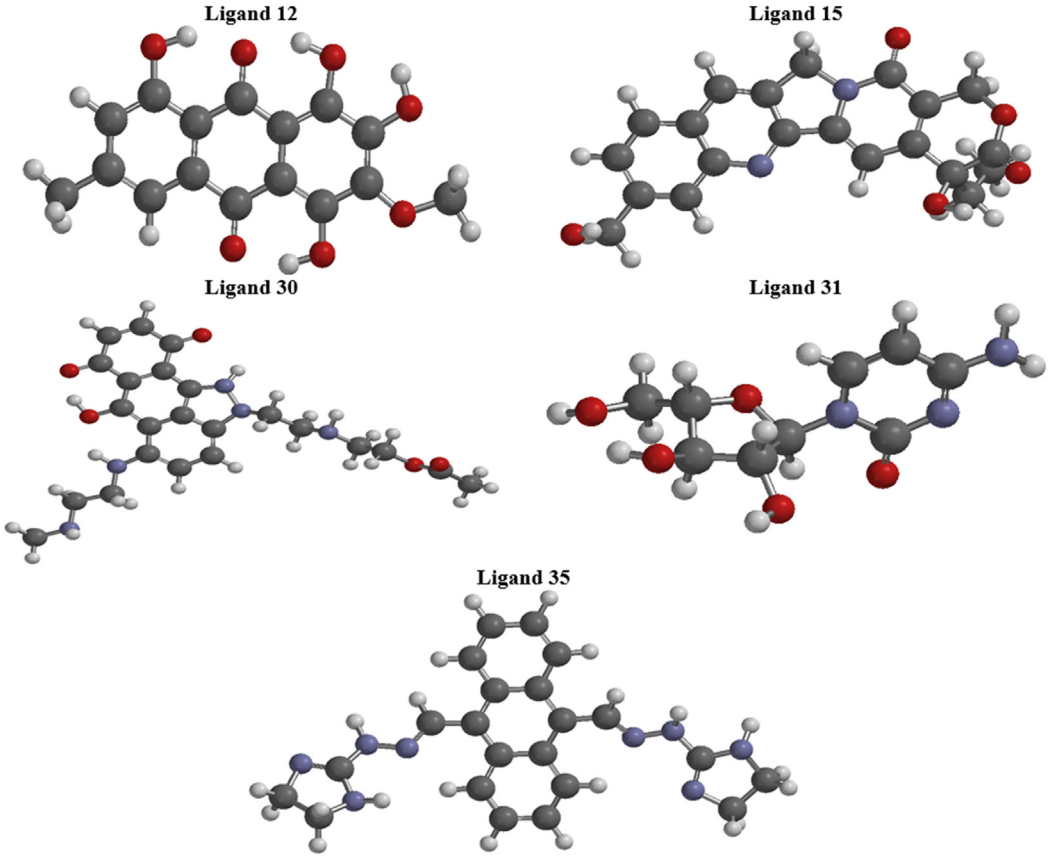

Figure 8: Optimized-geometric structures of the investigated ligands (12, 15, 30, 31, and 35).

best five ligands as well as vemurafenib, and the types of interactions involved in each of the selected complexes, are presented in Tables 1 and 2. Figures 2–7 depict the 3D and 2D interaction models of the selected docked ligands at the *V600E-BRAF* binding site. To further confirm that the selected compounds were potential drugs, we determined their drug likeness and pharmacokinetics. The predicted drug likeness and pharmacokinetic properties are shown in Tables 3 and 4. The optimized geometries and the frontier molecular orbitals (HOMO and LUMO illustrations) of the selected ligands, achieved through DFT computations, are shown in Figures 8 and 9. Table 5 shows the quantum descriptors, and Figure 10 depicts the EP surfaces of the studied ligands.

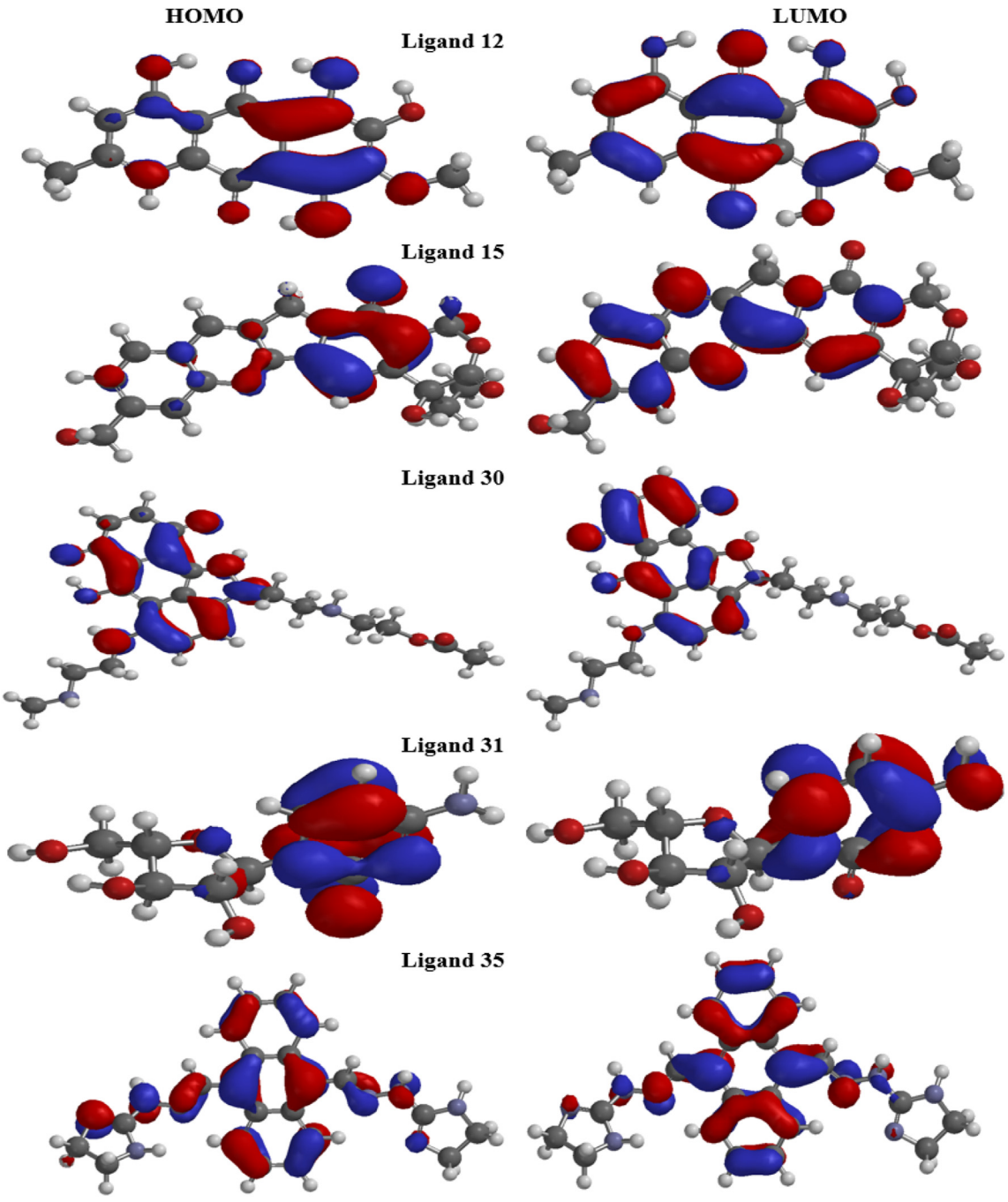

Figure 9: Frontier molecular orbital surfaces of the investigated ligands (12, 15, 30, 31, and 35).

Table 5: Frontier molecular orbital energies and global reactivity descriptors of the studied ligands.

S/N	E-HOMO (eV)	E-LUMO (eV)	ΔE	η	σ	χ	M	ω
12	−5.85	−2.90	2.95	1.48	0.68	4.38	−4.38	6.49
15	−5.97	−2.29	3.68	1.84	0.54	4.13	−4.13	4.64
30	−4.54	−2.56	1.98	0.99	1.01	3.55	−3.55	6.36
31	−6.02	−0.79	5.23	2.62	0.38	3.41	−3.41	2.22
35	−4.94	−2.15	2.79	1.40	0.72	3.55	−3.55	4.50

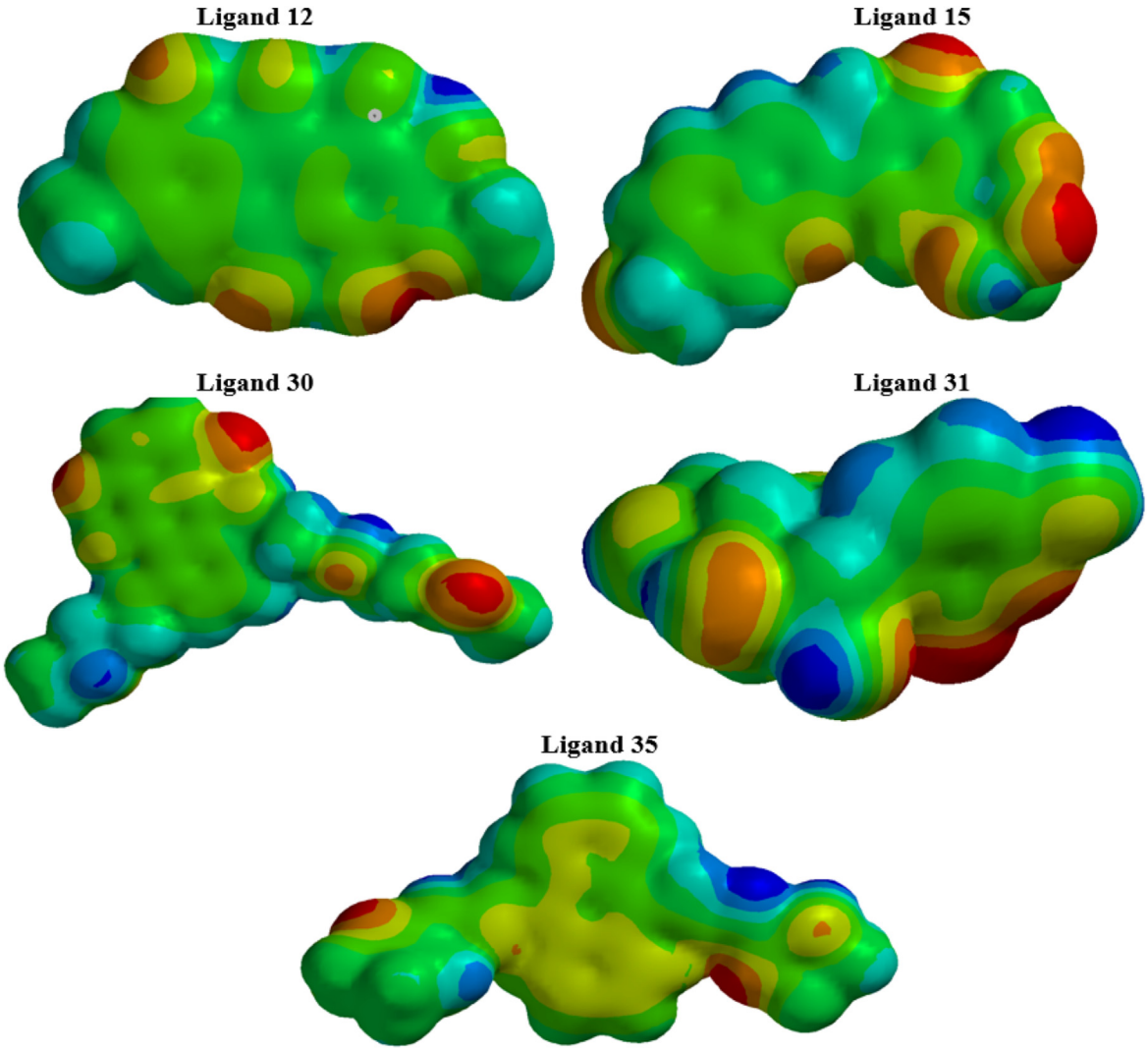

Figure 10: Electrostatic potential of the studied ligands (12, 15, 30, 31, and 35).

Discussion

Potential hit molecules were identified by docking all curated ligands from the PubChem database, including vemurafenib, into the binding pocket of the *V600E-BRAF* target. Before the docking was performed for the entire data set, the docking method was authenticated through a re-docking technique. Thus, vemurafenib (co-crystallized) was re-docked at the exact site where the co-crystal ligand was initially bound to the *V600E-BRAF* kinase. Re-docking of vemurafenib at the *V600E-BRAF* kinase receptor revealed an RMSD value of 1.413 Å, which met the validity standards of RMSD <2.0 Å.[36] Hence, the docking procedure with MVD had acceptable precision in repositioning vemurafenib at the *V600E-BRAF* active sites. The superimposed alignment of the re-docked and actual co-crystal structures is shown in Fig. S1. The coordinates for the active site and the grid box size used in the established re-docking procedure were also used for docking of the studied compounds. The top inhibitors of *V600E-BRAF* were sorted according to docking score with respect to that of vemurafenib (reference), and the selected ligands were found to efficiently bind the target.

To provide superior performance with outstanding docking scores, we examined the molecular interactions of the five hit inhibitors from the data set. The identification of the main residues in the binding pocket of the *V600E-BRAF* interacting with the five selected complexes (12, 15, 30, 31, and 35) was achieved with Discovery-Studio Visualizer. The potency of the interaction between the ligands and protein was assessed with the Rerank score. The complete docking results for the best five ligands as well as vemurafenib are presented in Table 1. Figures 2–7 show the 3D and 2D interaction models of the selected docked poses in the binding site of *V600E-BRAF*. Table 2 presents the interaction types involved in each of the selected complexes. The selected ligands formed bonds and non-bonding interactions with the binding pocket of the *V600E-BRAF* target, as indicated by the inter-energy and H-bonding energy (Table 1). All ligands had a MolDock score <-90 kcalmol^{-1}, thus indicating their potential to bind the

protein efficiently.[37] The complex structures of the five best poses, on the basis of the docking scores, are discussed in detail below and presented in Figures 2–7.

The complex structure of docked compound 12 with the target is shown in Figure 2. A MolDock score of −139.140 kcal mol^{-1} and Rerank score of −106.737 were determined. The E−H-bond was −8.202 kcal mol^{-1} (Table 1). The good docking scores suggested the potential for desirable interactions between this compound and the protein. The indicated binding mode in Figure 2 indicated that compound 12 establishes interactions through H-bonding with the backbone of the central amino acid residues CYS532 and GLN530; and shows favorable π−π interactions with the TRP531 and PHE583 residues, which are important for selectivity.[38] Additionally, compound 12 forms π−alkyl interactions with VAL471, ALA481, LEU514, and CYS532 (2) at the binding cavity, in a similar pattern to that reported in the literature.[25]

Figure 3 depicts the binding mode of compound 15 on the *V600E-BRAF* receptor, with MolDock, and Rerank scores of −123.093 kcal mol^{-1} and −93.530, respectively, and E−H-bond of −5.170 kcal mol^{-1} (Table 1). Compound 15 binds the *V600E-BRAF* binding cavity through three H-bonds with ASP594, CYS532, and GLU533, one C−H-bond with ASP594, and two π−π stacked interactions with TRP531 and PHE583 residues. A π−sigma interaction with CYS532 is also formed. Furthermore, the good docking score of compound 15 might be associated with other weak interactions: alkyl with VAL471, and π−alkyl interactions with the TRP531, PHE583, VAL471, ALA481, LYS483, LEU514, ALA481, and CYS532 residues. The 3D protein surface in Figure 3 suggested that compound 15 has a high affinity toward the target.

The docked structure of compound 30 with the receptor (Figure 4) had good MolDock and Rerank scores of −147.599 kcal mol^{-1} and −115.756, respectively, and E−H-bond of −4.770 kcal mol^{-1} (Table 1). These findings demonstrated that a stable interaction between this molecule and the receptor was possible. LYS483 and ALA481 were identified to form H-bonds with *V600E-BRAF*. For compound 30, similarly to vemurafenib (Figure 7), the benzene ring moiety intercalates in the space, thus forming four π−π interactions with TRP531 and PHE583 (3). The complex's stability may be associated with an additional alkyl interaction and π−alkyl interactions with the VAL471, ALA481, VAL471, ALA481, and CYS532 residues.

Figure 5 depicts the complex structure of compound 31 docked with the receptor. The MolDock and Rerank scores of −101.144 kcal mol^{-1} and −76.975, respectively, and E−H-bond of −9.939 kcal mol^{-1} (Table 1) indicated the possibility of good interactions between this molecule and the receptor. The LYS483, ASP594 (2), PHE595, GLY596, THR508, LEU514, and THR529 residues form four H-bonds between the molecule and the receptor. In addition, one C−H-bond forms with LYS483. Additional π−alkyl interactions with LEU505 and LEU514 residues may contribute to the complex's stability.

Compound 35 docked in the binding site of *V600E-BRAF* (Figure 6) had a high docking score (Table 1), thus indicating its binding in the binding site of one of the protomers in the protein dimer via two H-bonds with GLY534 and CYS532 residues. One H-bond forms between the N-atom of the imidazole ring and GLY534, and the other forms between the N atom of the −NH linker and the CYS532 residue. Seven C−H bonds were also observed with the LYS483, GLY534, ILE527, ALA481 (2), THR529, and ILE527 residues. Furthermore, three π−π stacked interactions were observed between the active site of the target residues TRP531 and PHE583 and compound 35, owing to aromatic ring intercalation (Figure 6). Additional π−alkyl interactions with five residues (VAL471 (2), ALA481, LEU514, and CYS532) were observed.

H-bonding is a unique sign of robust interactions between proteins and ligands, and typically results in elevated binding affinity.[39] In such interactions, the number of H-bonds usually increases the inhibitory potential toward the target. As indicated in Figures 2–7, which show 3D and 2D models of the interaction modes in the target binding site, the appearance of conventional H-bonds between the selected ligands and the anticancer receptor resulted in suitable ligand binding. Vemurafenib, as a standard for comparison with the investigated ligands, was docked into the same protein, and all selected ligands were found to outperformed vemurafenib. Notably, the investigated ligands inhibited the melanoma target in a pattern similar to that of vemurafenib. Some selected ligands had higher E−H-bond scores than vemurafenib.

Drug likeness and pharmacokinetic investigations of the investigated ligands were performed through the SwissADME and pkCSM web servers[40,41] (Tables 3 and 4). Lipinski's rule[42] suggests that good absorption occurs only at a molecular weight <500 g mol^{-1}, with fewer than five H bond donors, log P < 5, and fewer than 10 H bond acceptors. Table 3 shows that the molecular weights of the investigated compounds were in the range of 453.49 to 243.22 $gmol^{-1}$; therefore, the selected compounds were within the permissible range of Lipinski's rule. Moreover, none of the studied compounds had more than 10 H-bond acceptors; the highest number was seven for ligands 12 and 30. In addition, the selected ligands had fewer than five H-bond donors. The value for log P was <5 for all selected ligands. Veber's rule[43] recommends that the TPSA should be < 140 $Å^2$ and that the TPSA of the selected ligands should not be >137.48 $Å^2$. Veber has also proposed that the NRB in the ligand should not exceed 10. According to the results in Table 3, all ligands examined in this study had the highest NR of 6 with only ligand 30 that have 11, which agrees with the Veber's rule. The selected ligands were further filtered for an optimum permeability and bioavailability profile according to bioavailability score (ABS) standards. An ABS score of 0.55 implies compliance with Lipinski's rule.[42]

The intestinal absorption of the selected ligands had values above 50%, thus demonstrating their ease of absorption. VDss indicates a volume distribution in a stable state, thus demonstrating uniform distribution of the drug to all tissues. A VDss value >0.5 suggests that a drug candidate is sufficiently distributed in the plasma, whereas a value below−0.5 indicates that a drug has a low ability to cross the cell membrane. The VDss were in the range of 1.900 to−0.445, thus indicating that the investigated ligands had adequate distribution in the plasma. In addition, the blood−

brain barrier (BBB) and central nervous system (CNS) penetrability are essential factors that must be considered for acquiring optimal pharmacological drugs. The BBB and CNS penetrability standard values were to >0.3 for log blood brain (BB), and <−3 to >−2 for log PS. In a given ligand, log BB <−1 indicates insufficient diffusion of the drug molecule to the brain, and log BB >0.3 indicates that the drug molecule can cross the BBB; a log PS value >−2 indicates that the drug molecule can enter the CNS, whereas a value <−3 suggests that the drug molecule cannot easily reach the CNS.[44] The results in Table 4 revealed that the selected ligands demonstrated a high possibility of crossing these barriers.

Cytochrome (CYP450), a major metabolic enzyme in the human body, has five main isoforms: CYPA2, CYP2C19, CYP2C9, CYP2D6, and CYP3A4. The results in Table 4 indicated promising inhibition ability toward the enzymes, with safe pharmacokinetic interactions. The dosing effect and bioavailability of a drug to reach the required concentrations is determined by the clearance. Low clearance suggests persistence of a drug molecule in the body. All selected ligands demonstrated good acceptability in the body. Toxicity is used to decide whether a drug candidate is toxic. As shown in Table 4, ligands 12, 15, 30, and 31 were non-toxic. Consequently, the selected ligands had favorable pharmacokinetic properties and might be used as *V600E-BRAF* inhibitors in the future.

The geometry-optimized structures of the selected ligands from DFT computations are shown in Figure 8. All geometry-optimized structures conformed to a global minimum. The frontier molecular orbitals (HOMO and LUMO) of the five best ligands indicated a crucial role in charge−transfer interactions between the ligand and the target's active site. In Figure 9, the blue and red colors indicate the positive and negative regions of the orbital.[45] Additionally, the shapes of the frontier orbitals can be used as a guide for determining reactivity. In every ligand, the HOMO is delocalized onto the π-bonds. According to the pattern, the blue area denotes the highest value of HOMO, whereas the red area denotes the lowest value.[46] The HOMO electron-density distribution of the investigated ligands indicated promising interactions of the ligands with *V600E-BRAF*. Similarly, the LUMO delocalized over several areas of the aryl ring of the ligands. Nonetheless, the conjugated bonds and hetero-atoms made to the binding interaction with the target. The HOMO and LUMO electronic surfaces indicated that the π-bonds and hetero-atoms interact with the target under favorable conditions. This typical behavior is suitable for donor-acceptor interactions which may be responsible for the excellent binding of the ligands to the *V600E-BRAF*.

Table 5 displays the energies of the HOMO and LUMO, including quantum chemical descriptors associated with the studied ligands. A good electron-donor molecule has a high HOMO energy, whereas a lower energy value indicates a weak electron acceptor.[47] In addition, a low energy gap (LUMO−HOMO) substantially affects intermolecular charge transfer and molecule bioactivity. Consequently, the small energy gap observed in the hit ligands positively affected electron movement from the HOMO to the LUMO, thus resulting in a strong affinity of the inhibitor for *V600E-BRAF*. The Egap value increased as follows: 30 (1.98 eV) > 35 (2.79 eV) > 12 (2.95 eV) > 15 (3.68 V) > 31 (5.23 eV). Hence, the reactivity order increased, and the most reactive value was 30 (1.98 eV). The order of the reactivity increase matched the decreases in energy gap values.

The η (hardness) and σ (softness) are important reactivity variables for the performance of a ligand in a chemical system. Hard molecules have higher resistance to alteration of their electronic-dispersal during a chemical reaction, whereas soft molecules have lower resistance to alteration of the distribution of their electrons in a reaction.[48,49] The results in Table 5 indicated high η and low σ values with respect to those of analogous reported molecules.[50] The χ (electronegativity) of a molecule determines its electron-attraction capability.[51] The χ was computed to be approximately 3.41−4.38 eV, describing the studied ligands as donor-electrons. The μ (chemical potential) had negative values for all studied ligands, which implies good stability, and the formation of a stable complex with the receptor. The ω (electrophilicity) of a molecule predicts the electrophilic nature and measures the tendency to accept an electron. Organic molecules' ω values are classified as follows: ω < 0.8 eV indicates weak electrophiles; ω between 0.8 and 1.5 eV indicates moderate electrophiles; and ω > 1.5 eV indicates strong electrophiles.[52] The computed ω for the studied ligands indicated that they were good electrophiles. Ligands with a high ω value have potential anticancer activity.[53,54] Finally, comparison of the orbital energies (eV), global reactivity variables, and docking scores of the best four ligands from the data set indicated that the selected ligands may be considered potential *V600E-BRAF* inhibitors with desirable properties.

The molecular electrostatic-potential (MEP) surface designates the charge distribution, thus providing a good understanding of the physical and chemical properties of a molecule. The MEP predicts the electrophilic and nucleophilic active sites of a given molecule.[45,54] When the point of charge is located in an area of surplus positive charge, the point charge ligand interaction becomes repulsive, and the EP therefore is positive. However, if the point of charge is situated in a region of a surplus negative charge, then an attractive interaction occurs, and the EP becomes negative.[55,56] The MEP maps of the selected ligands are presented in Figure 10; red color shows the nucleophilic region, blue color indicates the electrophilic region, and intermediate colors indicate moderate values of MEP. Thus, the increase follows the order red < orange < yellow < green < blue.[57] In most cases, the negative charges are situated on the O-atoms, and the positive areas of the molecules are the areas where the H-atoms bonded to O-atoms are situated. The positive and negative cores of the selected molecules participate in forming interactions with both bonded and non-bonded (particularly H-bonds) areas in the complexes during docking.[58]

Future research should include molecular dynamic simulations of the selected compounds to further investigate their ability to induce confrontational changes in the *V600E-BRAF* kinase. In addition, new molecules should be designed from the selected hit molecules, synthesized, and tested in vivo and in vitro, to establish their potency as *V600E-BRAF* inhibitors for the treatment of melanoma and other *V600E-BRAF* related cancers.

Conclusions

Molecular docking simulation, pharmacokinetic evaluation, and DFT computations were successfully performed to determine potential hit compounds against *V600E-BRAF* from a series of 72 anticancer compounds from the PubChem database. The five top-ranked compounds (12, 15, 30, 31, and 35) were identified to have excellent docking scores in the active site of the *V600E-BRAF* target. The docking results indicated that both hydrophobic interactions and H bonds play major roles in the binding interactions of the potential compounds with *V600E-BRAF*. The predicted physicochemical and pharmacokinetic parameters were in acceptable ranges for drug screening criteria. The quantum chemical parameters computed with the DFT approach indicated that the selected molecules have stable structures and are highly electrophilic, whereas the distribution of the MEP identified the potential sites for nucleophilic and electrophilic attack. The broad computational investigations indicated that the selected molecules may be considered potential hits against the *V600E-BRAF* target and may be promising as anticancer agents.

Source of funding

This work was fully sponsored by the Tertiary Education Trust Fund (TETFUND), grant number TETF/DR&D/UNI/ZARIA/IBR/2020/VOL./54.

Conflict of interest

The authors have no conflict of interest to declare.

Ethical approval

This research was fully sponsored by the Tertiary Education Trust Fund (NG) under IBR Project grant 2020 with project number TETF/DR&D/UNI/ZARIA/IBR/2020/VOL./54 dated 21st February, 2022.

Consent

Not relevant.

Authors' contributions

ABU: Designed and performed the study, interpreted the results, and wrote the manuscript. AU: Contributed to designing the study, and supervised and edited the manuscript. All authors have critically reviewed and approved the final draft and are responsible for the content and similarity index of the manuscript.

Acknowledgments

We thank the TETFUND for the 2020 Institution-Based Research project grant (TETF/DR&D/UNI/ZARIA/IBR/2020/VOL.1/54) for this study.

Appendix A. Supplementary data

Supplementary data to this article can be found online at https://doi.org/10.1016/j.jtumed.2023.01.013.

References

1. Li Z-L, Prakash P, Buck M. *A "tug of war"* maintains a dynamic protein–membrane complex: molecular dynamics simulations of C-Raf RBD-CRD bound to K-Ras4B at an anionic membrane. **ACS Cent Sci 2018**; 4(2): 298–305.
2. Liu Z, Wang M, Wang H, Fang L, Gou S. Platinum-based modification of styrylbenzylsulfones as multifunctional antitumor agents: targeting the RAS/RAF pathway, enhancing antitumor activity, and overcoming multidrug resistance. **J Med Chem 2019**; 63(1): 186–204.
3. Wang P-F, Qiu H-Y, Wang Z-F, Zhang Y-J, Wang Z-C, Li D-D, et al. Identification of novel B-RafV600E inhibitors employing FBDD strategy. **Biochem Pharmacol 2017**; 132: 63–76.
4. Wang ZF, Wang PF, Ma JT, Chai YZ, Hu HM, Gao WL, et al. Design of potent B-RafV600E inhibitors by multiple copy simulation search strategy. **Chem Biol Drug Des 2018**; 91(2): 567–574.
5. Umar BA, Uzairu A, Shallangwa GA, Uba S. Rational drug design of potent V600E-BRAF kinase inhibitors through molecular docking simulation. **J Eng Exact Sci 2019**; 5(5): 469–481.
6. McCubrey JA, Steelman LS, Abrams SL, Lee JT, Chang F, Bertrand FE, et al. Roles of the RAF/MEK/ERK and PI3K/PTEN/AKT pathways in malignant transformation and drug resistance. **Adv Enzym Regul 2006**; 46(1): 249–279.
7. Chappell WH, Steelman LS, Long JM, Kempf RC, Abrams SL, Franklin RA, et al. Ras/Raf/MEK/ERK and PI3K/PTEN/Akt/mTOR inhibitors: rationale and importance to inhibiting these pathways in human health. **Oncotarget 2011**; 2(3): 135.
8. Yang H, Higgins B, Kolinsky K, Packman K, Go Z, Iyer R, et al. RG7204 (PLX4032), a selective BRAFV600E inhibitor, displays potent antitumor activity in preclinical melanoma models. **Cancer Res 2010**; 70(13): 5518–5527.
9. Blasco RB, Francoz S, Santamaría D, Cañamero M, Dubus P, Charron J, et al. c-Raf, but not B-Raf, is essential for development of K-Ras oncogene-driven non-small cell lung carcinoma. **Cancer Cell 2011**; 19(5): 652–663.
10. Qin J, Xie P, Ventocilla C, Zhou G, Vultur A, Chen Q, et al. Identification of a novel family of BRAFV600E inhibitors. **J Med Chem 2012**; 55(11): 5220–5230.
11. Wang P-F, Zhang Y-J, Wang D, Hu H-M, Wang Z-C, Xu C, et al. Design, synthesis, and biological evaluation of new B-RafV600E kinase inhibitors. **Bioorg Med Chem 2018**; 26(9): 2372–2380.
12. Brose MS, Volpe P, Feldman M, Kumar M, Rishi I, Gerrero R, et al. BRAF and RAS mutations in human lung cancer and melanoma. **Cancer Res 2002**; 62(23): 6997–7000.
13. Long GV, Stroyakovskiy D, Gogas H, Levchenko E, de Braud F, Larkin J, et al. Combined BRAF and MEK inhibition versus BRAF inhibition alone in melanoma. **N Engl J Med 2014**; 371(20): 1877–1888.
14. Ammar UM, Abdel-Maksoud MS, Oh C-H. Recent advances of RAF (rapidly accelerated fibrosarcoma) inhibitors as anticancer agents. **Eur J Med Chem 2018**; 158: 144–166.
15. Amin KM, El-Badry OM, Rahman DEA, Ammar UM, Abdalla MM. Design, synthesis, anticancer evaluation and molecular docking of new V600EBRAF inhibitors derived from pyridopyrazinone. **Eur J Chem 2016**; 7(1): 19–29.

16. Prahallad A, Sun C, Huang S, Di Nicolantonio F, Salazar R, Zecchin D, et al. Unresponsiveness of colon cancer to BRAF (V600E) inhibition through feedback activation of EGFR. **Nature 2012**; 483(7387): 100–103.
17. Akhtar MJ, Siddiqui AA, Khan AA, Ali Z, Dewangan RP, Pasha S, et al. Design, synthesis, docking and QSAR study of substituted benzimidazole linked oxadiazole as cytotoxic agents, EGFR and erbB2 receptor inhibitors. **Eur J Med Chem 2017**; 126: 853–869.
18. Regad T. Targeting RTK signaling pathways in cancer. **Cancers 2015**; 7(3): 1758–1784.
19. Wilhelm SM, Adnane L, Newell P, Villanueva A, Llovet JM, Lynch M. Preclinical overview of sorafenib, a multikinase inhibitor that targets both Raf and VEGF and PDGF receptor tyrosine kinase signaling. **Mol Cancer Therapeut 2008**; 7(10): 3129–3140.
20. Bryan MC, Falsey JR, Frohn M, Reichelt A, Yao G, Bartberger MD, et al. N-substituted azaindoles as potent inhibitors of Cdc7 kinase. **Bioorg Med Chem Lett 2013**; 23(7): 2056–2060.
21. Flaherty KT, Puzanov I, Kim KB, Ribas A, McArthur GA, Sosman JA, et al. Inhibition of mutated, activated BRAF in metastatic melanoma. **N Engl J Med 2010**; 363(9): 809–819.
22. Infante J, Fecher L, Nallapareddy S, Gordon M, Flaherty K, Cox D, et al. Safety and efficacy results from the first-in-human study of the oral MEK 1/2 inhibitor GSK1120212. **J Clin Oncol 2010**; 28(15_suppl): 2503. 2503.
23. Karthick T, Tandon P. Computational approaches to find the active binding sites of biological targets against busulfan. **J Mol Model 2016**; 22(6): 1–9.
24. Cumming JG, Davis AM, Muresan S, Haeberlein M, Chen H. Chemical predictive modelling to improve compound quality. **Nat Rev Drug Discov 2013**; 12(12): 948–962.
25. Umar AB, Uzairu A, Shallangwa GA, Uba S. Molecular docking strategy to design novel V600E-BRAF kinase inhibitors with prediction of their drug-likeness and pharmacokinetics ADMET properties. **Chem Africa 2020**: 1–17.
26. Deghady AM, Hussein RK, Alhamzani AG, Mera A. Density functional theory and molecular docking investigations of the chemical and antibacterial activities for 1-(4-Hydroxyphenyl)-3-phenylprop-2-en-1-one. **Molecules 2021**; 26(12): 3631.
27. Hussein R, Elkhair H. Molecular docking identification for the efficacy of some zinc complexes with chloroquine and hydroxychloroquine against main protease of COVID-19. **J Mol Struct 2021**; 1231:129979.
28. Opo FA, Rahman MM, Ahammad F, Ahmed I, Bhuiyan MA, Asiri AM. Structure based pharmacophore modeling, virtual screening, molecular docking and ADMET approaches for identification of natural anti-cancer agents targeting XIAP protein. **Sci Rep 2021**; 11(1): 1–17.
29. Umar BA, Uzairu A. In-silico approach to understand the inhibition of corrosion by some potent triazole derivatives of pyrimidine for steel. **SN Appl Sci 2019**; 1(11): 1413.
30. Bollag G, Hirth P, Tsai J, Zhang J, Ibrahim PN, Cho H, et al. Clinical efficacy of a RAF inhibitor needs broad target blockade in BRAF-mutant melanoma. **Nature 2010**; 467(7315): 596.
31. Choi W-K, El-Gamal MI, Choi HS, Baek D, Oh C-H. New diarylureas and diarylamides containing 1, 3, 4-triarylpyrazole scaffold: synthesis, antiproliferative evaluation against melanoma cell lines, ERK kinase inhibition, and molecular docking studies. **Eur J Med Chem 2011**; 46(12): 5754–5762.
32. Molegro A. *MVD 5.0 Molegro virtual docker*. Denmark: DK-8000 Aarhus C; 2011.
33. Wang G-m, Wang X, Zhu J-m, Guo B-b, Yang Z, Xu Z-j, et al. Docking-based structural splicing and reassembly strategy to develop novel deazapurine derivatives as potent B-Raf V600E inhibitors. **Acta Pharmacol Sin 2017**; 38(7): 1059–1068.
34. Thomsen R, Christensen MH. MolDock: a new technique for high-accuracy molecular docking. **J Med Chem 2006**; 49(11): 3315–3321.
35. Tsuneda T, Song J-W, Suzuki S, Hirao K. On Koopmans' theorem in density functional theory. **J Chem Phys 2010**; 133(17):174101.
36. Yusuf D, Davis AM, Kleywegt GJ, Schmitt S. An alternative method for the evaluation of docking performance: RSR vs RMSD. **J Chem Inf Model 2008**; 48(7): 1411–1422.
37. Abdullahi M, Uzairu A, Shallangwa GA, Arthur DE, Umar BA, Ibrahim MT. Virtual molecular docking study of some novel carboxamide series as new anti-tubercular agents. **Eur J Chem 2020**; 11(1): 30–36.
38. Hassan AH, Lee K-T, Lee YS. Flavone-based arylamides as potential anticancers: design, synthesis and in vitro cell-based/cell-free evaluations. **Eur J Med Chem 2020**; 187:111965.
39. Khan IM, Islam M, Shakya S, Alam N, Imtiaz S, Islam MR. Synthesis, spectroscopic characterization, antimicrobial activity, molecular docking and DFT studies of proton transfer (H-bonded) complex of 8-aminoquinoline (donor) with chloranilic acid (acceptor). **J Biomol Struct Dyn 2021**: 1–15.
40. Daina A, Michielin O, Zoete V. SwissADME: a free web tool to evaluate pharmacokinetics, drug-likeness and medicinal chemistry friendliness of small molecules. **Sci Rep 2017**; 7:42717.
41. Pires DE, Blundell TL, Ascher DB. pkCSM: predicting small-molecule pharmacokinetic and toxicity properties using graph-based signatures. **J Med Chem 2015**; 58(9): 4066–4072.
42. Lipinski CA, Lombardo F, Dominy BW, Feeney PJ. Experimental and computational approaches to estimate solubility and permeability in drug discovery and development settings. **Adv Drug Deliv Rev 1997**; 23(1–3): 3–25.
43. Veber DF, Johnson SR, Cheng H-Y, Smith BR, Ward KW, Kopple KD. Molecular properties that influence the oral bioavailability of drug candidates. **J Med Chem 2002**; 45(12): 2615–2623.
44. Clark DE. In Silico prediction of blood–brain barrier permeation. **Drug Discov Today 2003**; 8(20): 927–933.
45. Khattab M, Al-Karmalawy AA. Revisiting activity of some nocodazole analogues as a potential anticancer drugs using molecular docking and DFT calculations. **Front Chem 2021**; 9: 628398.
46. Celik S, Akyuz S, Ozel AE. Structural and vibrational investigations and molecular docking studies of a vinca alkoloid, vinorelbine. **J Biomol Struct Dyn 2022**: 1–20.
47. Manoj K, Elangovan N, Chandrasekar S. Synthesis, XRD, hirshfeld surface analysis, ESP, HOMO-LUMO, quantum chemical modeling and anticancer activity of di (p-methyl benzyl)(dibromo)(1, 10-phenanthroline) tin (IV) complex. **Inorg Chem Commun 2022**; 139:109324.
48. Murulana LC, Singh AK, Shukla SK, Kabanda MM, Ebenso EE. Experimental and quantum chemical studies of some bis (trifluoromethyl-sulfonyl) imide imidazolium-based ionic liquids as corrosion inhibitors for mild steel in hydrochloric acid solution. **Ind Eng Chem Res 2012**; 51(40): 13282–13299.
49. Wazzan NA. DFT calculations of thiosemicarbazide, arylisothiocynates, and 1-aryl-2, 5-dithiohydrazodicarbonamides as corrosion inhibitors of copper in an aqueous chloride solution. **J Ind Eng Chem 2015**; 26: 291–308.
50. Fahim AM, Farag AM. Synthesis, antimicrobial evaluation, molecular docking and theoretical calculations of novel pyrazolo [1, 5-a] pyrimidine derivatives. **J Mol Struct 2020**; 1199: 127025.
51. Karton A, Spackman PR. Evaluation of density functional theory for a large and diverse set of organic and inorganic equilibrium structures. **J Comput Chem 2021**; 42(22): 1590–1601.
52. Edim MM, Enudi OC, Asuquo BB, Louis H, Bisong EA, Agwupuye JA, et al. Aromaticity indices, electronic structural

properties, and fuzzy atomic space investigations of naphthalene and its aza-derivatives. **Heliyon 2021**; 7(2):e06138.
53. Srivastava R. Theoretical studies on the molecular properties, toxicity, and biological efficacy of 21 new chemical entities. **ACS Omega 2021**; 6(38): 24891−24901.
54. El-Bindary MA, El-Desouky MG, El-Bindary AA. Metal−organic frameworks encapsulated with an anticancer compound as drug delivery system: synthesis, characterization, antioxidant, anticancer, antibacterial, and molecular docking investigation. **Appl Organomet Chem 2022**; 36(5):e6660.
55. Celik S, Vagifli F, Akyuz S, Ozkok F, Ozel AE, Dosler S, et al. Synthesis, vibrational spectroscopic investigation, molecular docking, antibacterial and antimicrobial studies of a new anthraquinone derivative compound. **Spectrosc Lett 2022**: 1−19.
56. Singh P, Islam S, Ahmad H, Prabaharan A. Spectroscopic investigation (FT-IR, FT-Raman), HOMO-LUMO, NBO, and molecular docking analysis of N-ethyl-N-nitrosourea, a potential anticancer agent. **J Mol Struct 2018**; 1154: 39−50.
57. Balachandran V, Karpagam V, Revathi B, Kavimani M, Ilango G. Conformational stability, spectroscopic and computational studies, HOMO−LUMO, NBO, ESP analysis, thermodynamic parameters of natural bioactive compound with anticancer potential of 2-(hydroxymethyl) anthraquinone. **Spectrochim Acta Mol Biomol Spectrosc 2015**; 150: 631−640.
58. Jordaan MA, Ebenezer O, Damoyi N, Shapi M. Virtual screening, molecular docking studies and DFT calculations of FDA approved compounds similar to the non-nucleoside reverse transcriptase inhibitor (NNRTI) efavirenz. **Heliyon 2020**; 6(8):e04642.

How to cite this article: Umar AB, Uzairu A. **Virtual screening, pharmacokinetic, and DFT studies of anticancer compounds as potential *V600E-BRAF* kinase inhibitors**. J Taibah Univ Med Sc 2023;18(5):933−946.